Biochemical and Biophysical Research Communications 453 (2014) 43–48

Contents lists available at ScienceDirect

Biochemical and Biophysical Research Communications

journal homepage: www.elsevier.com/locate/ybbrc

Mutation in the β-hairpin of the *Bordetella pertussis* adenylate cyclase toxin modulates N-lobe conformation in calmodulin

Tzvia I. Springer [a], Erich Goebel [a], Dinesh Hariraju [a], Natosha L. Finley [a,b,*]

[a] Department of Microbiology, Miami University, Oxford, OH 45056, USA
[b] Cell, Molecular, and Structural Biology Program, Miami University, Oxford, OH 45056, USA

ARTICLE INFO

Article history:
Received 26 August 2014
Available online 22 September 2014

Keywords:
Adenylate cyclase
CyaA
Calmodulin
CaM
Molecular mechanism
NMR spectroscopy

ABSTRACT

Bordetella pertussis, causative agent of whooping cough, produces an adenylate cyclase toxin (CyaA) that is an important virulence factor. In the host cell, the adenylate cyclase domain of CyaA (CyaA-ACD) is activated upon association with calmodulin (CaM), an EF-hand protein comprised of N- and C-lobes (N-CaM and C-CaM, respectively) connected by a flexible tether. Maximal CyaA-ACD activation is achieved through its binding to both lobes of intact CaM, but the structural mechanisms remain unclear. No high-resolution structure of the intact CaM/CyaA-ACD complex is available, but crystal structures of isolated C-CaM bound to CyaA-ACD shed light on the molecular mechanism by which this lobe activates the toxin. Previous studies using molecular modeling, biochemical, and biophysical experiments demonstrate that CyaA-ACD's β-hairpin participates in site-specific interactions with N-CaM. In this study, we utilize nuclear magnetic resonance (NMR) spectroscopy to probe the molecular association between intact CaM and CyaA-ACD. Our results indicate binding of CyaA-ACD to CaM induces large conformational perturbations mapping to C-CaM, while substantially smaller structural changes are localized primarily to helices I, II, and IV, and the metal-binding sites in N-CaM. Site-specific mutations in CyaA-ACD's β-hairpin structurally modulate N-CaM, resulting in conformational perturbations in metal binding sites I and II, while no significant structural modifications are observed in C-CaM. Moreover, dynamic light scattering (DLS) analysis reveals that mutation of the β-hairpin results in a decreased hydrodynamic radius (R_h) and reduced thermal stability in the mutant complex. Taken together, our data provide new structural insights into the β-hairpin's role in stabilizing interactions between CyaA-ACD and N-CaM.

1. Introduction

The CyaA secreted by *Bordetella pertussis* influences bacterial pathogenesis in respiratory infections. CyaA is a 188 kDa protein composed of the C-terminal domain, which is necessary for interaction with host cell receptors, and the N-terminal domain, that is an adenylate cyclase toxin (CyaA-ACD) that is inserted through the membrane into the host cell cytosol [1]. Upon interaction with CaM, CyaA-ACD is activated and intracellular cyclic adenosine monophosphate concentration increases to pathophysiological levels, which is known to impair the host immune response [1–4]. CaM has four metal binding sites and is known to engage numerous effector proteins in response to calcium (Ca^{2+}) stimulation. Isolated N-CaM or C-CaM triggers CyaA-ACD activity, but association with intact CaM promotes a 400 fold increase in binding affinity and activation by unknown mechanisms emphasizing the importance of intermolecular associations between N-CaM and CyaA-ACD [5].

Structural and functional comparisons between CyaA-ACD and another CaM-dependent adenylate cyclase toxin from *Bacillus anthracis* (EF), reveal that distinct molecular mechanisms have evolved for the activation of these two enzymes [6–10]. In direct contrast to CyaA-ACD, EF requires both high levels of Ca^{2+} and interaction with intact CaM for full activation [11]. EF forms an extended complex such that the N-CaM makes extensive contacts with the helical domain of EF that stabilize the catalytic loop. CyaA-ACD lacks the helical domain, but association between the C-tail of CyaA-ACD and C-CaM stabilizes its catalytic loop. While crystal structures of C-CaM bound to CyaA-ACD reveal the mode

Abbreviations: CyaA, adenylate cyclase toxin; CyaA-ACD, adenylate cyclase domain; CaM, calmodulin; CyaA-ACD(Q260C), Gln260Cys mutant of CyaA-ACD; CyaA-ACD(R262A), Arg262Ala mutant of CyaA-ACD; TROSY, Transverse Relaxation Optimized Spectroscopy; HSQC, heteronuclear single quantum coherence.

* Corresponding author at: Department of Microbiology, Miami University, 700 East High Street, 32 PSN, Oxford, OH 45056, USA. Fax: +1 513 529 2431.
E-mail address: finleynl@miamioh.edu (N.L. Finley).

http://dx.doi.org/10.1016/j.bbrc.2014.09.048
0006-291X/

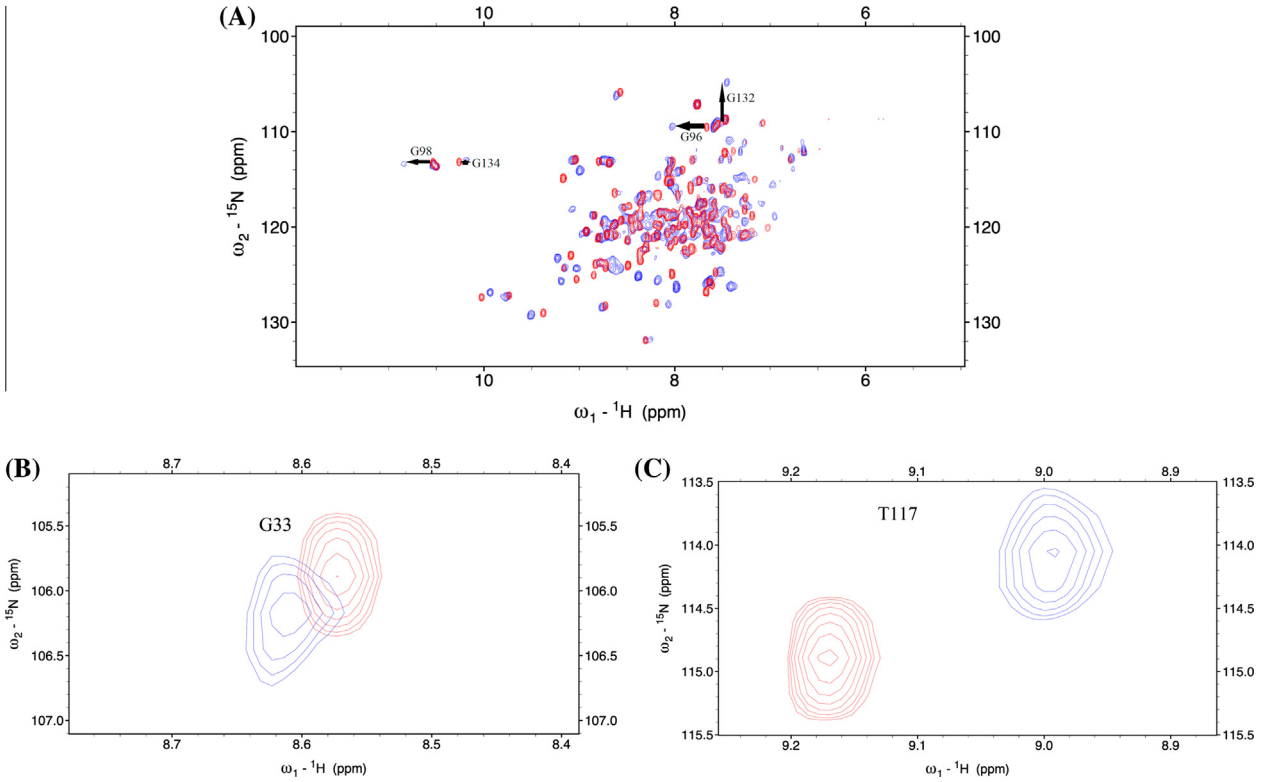

Fig. 1. Monitoring the association of CyaA with CaM by NMR. (A) Two dimensional ^{1}H–^{15}N TROSY-HSCQ spectrum of [^{2}H, ^{15}N, ^{13}C] CaM free (red) overlaid with [^{2}H, ^{15}N, ^{13}C] CaM/CyaA-ACD (blue). (B) Relatively small chemical shift perturbations are observed in N-CaM in the presence of CyaA-ACD supporting that this region likely binds the toxin with lower affinity. (C) However, residues mapping to the C-lobe of CaM, such as T117 in the F-G loop of CaM, experience larger chemical shift perturbation upon interaction with CyaA-ACD suggesting that this domain is involved in higher affinity interactions with the toxin. (For interpretation of the references to color in this figure legend, the reader is referred to the web version of this article.)

by which it likely controls CyaA-ACD function, no structural information is available detailing the role of N-CaM in toxin activation. CaM mutants defective in N-terminal opening stimulate CyaA-ACD, suggesting domain opening is not necessary for maximal activation [9]. Biochemical and molecular modeling studies showed that interaction between N-CaM and the β-hairpin (residues 259–273) of CyaA-ACD likely promotes full activation via conformational modulation of the catalytic pocket [9], but the mechanism remains to be determined. Here, we investigate the molecular interactions occurring between intact CaM and CyaA-ACD using NMR and DLS experiments. Our findings are interpreted within the context of the available structural data and the role of N-CaM interaction in CyaA-ACD activation is discussed.

2. Materials and methods

2.1. Protein expression, purification, and complex formation

The gene encoding 373-residues of CyaA-ACD (generously provided by Dr. Wei-Jen Tang, University of Chicago) was cloned into the pETite plasmid from the Expresso™ T7 expression system (Lucigen®). Mutation of Gln260Cys (CyaA-ACD(Q260C)) and Arg262Ala (CyaA-ACD(R262A)) in the CyaA-ACD gene was performed utilizing the Quikchange™ site-directed mutagenesis kit (Agilent). The recombinant CyaA-ACD, CyaA-ACD(Q260C), or CyaA-ACD(R262A) plasmid was transformed into separate *Escherichia coli* HI-Control BL21 (DE3) (Lucigen) cultures. Cells were grown in Luria–Bertani (LB) media containing 30 μg ml^{-1} kanamycin (kan) at 37 °C to A_{600} = 0.8–1.0 and protein production was induced by the addition of isopropyl-1-thiogalactopyranoside (IPTG) to a final concentration of 0.5 mM. Cells were harvested 20 h (h) post-induction by centrifugation.

Cell pellets containing CyaA-ACD, CyaA-ACD(Q260C), or CyaA-ACD(R262A) were re-suspended on ice in buffer containing 8 M Urea, 500 mM NaCl, 40 mM imidazole, 20 mM Tris–HCl and 1 mM phenylmethanesulfonylfluoride (PMSF) at pH 8.0 and lysed by sonication. The suspension was clarified by centrifugation at 16,000*g* for 30 min at 4 °C and the soluble supernatant was loaded onto a HisTrap™ HP Ni-Sepharose resin (GE Healthcare). The recombinant protein was eluted with increasing concentrations of imidazole and determined to be >95% homogeneous using sodium dodecyl sulfate polyacrylamide gel electrophoresis (SDS–PAGE) followed by Coomassie blue staining. Purified protein was pooled, the concentration was determined by Bradford assay, and stored at −20 °C.

The plasmid containing the gene encoding for human calmodulin (CaM) (a gift from Dr. Vadim Gaponenko, University of Illinois) was transformed into *E. coli* BL21 (DE3) (EMD Millipore). A single colony was grown in 5 ml LB media containing deuterium (^{2}H) oxide supplemented with 30 μg ml^{-1} kan at 37 °C to A_{600} = 0.5. Cells were harvested and re-suspended in M9 minimal media containing deuterium (^{2}H) oxide, ^{15}N-NH_4Cl, and $^{13}C_6$-Glucose (Sigma Aldrich) as the sole sources of nitrogen and carbon, respectively. Cells were grown to A_{600} = 0.8, induced with 0.5 mM IPTG, and harvested 20 h post-induction. CaM was purified in the presence of lysozyme and quantified as previously described [12]. Samples were concentrated using a centricon (CORNING) and stored at −20 °C.

For complex formation, CyaA-ACD, CyaA-ACD(Q260C), or CyaA-ACD(R262A) was refolded in the presence of equimolar CaM and dialyzed against 10 mM $CaCl_2$, 250 mM NaCl, 20 mM Hepes pH

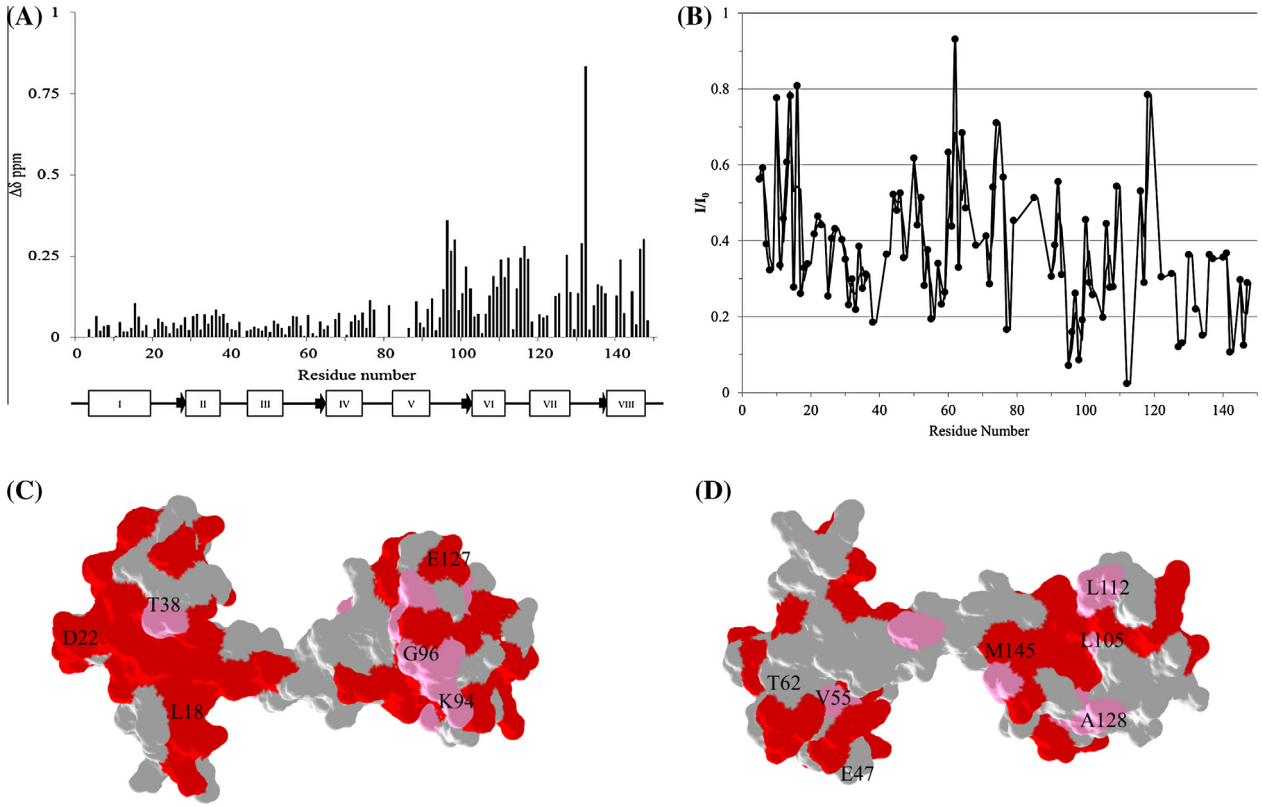

Fig. 2. CyaA-ACD binds both domains of CaM. (A) Composite amide proton and nitrogen chemical shift differences between [^{2}H, ^{15}N, ^{13}C] CaM free and [^{2}H, ^{15}N, ^{13}C] CaM/CyaA-ACD show the regions of CaM structurally perturbed upon CyaA-ACD association. Secondary structural elements are depicted below the graph as helices (rectangles) and sheets (arrows). (B) The ratios of the CaM amide-proton–nitrogen resonances in the presence (I) and absence of CyaA-ACD (I_o) were determined and normalized to 1 for the largest value observed (T62 in N-CaM). (C) and (D) Residues with peak ratios between 0 and 0.19 and 0.20 and 0.45 were colored-coded pink and red on the Ca^{2+}-saturated CaM crystal structure (1CLL); all overlapping and residues with peak ratios above 0.45 were colored grey. (For interpretation of the references to color in this figure legend, the reader is referred to the web version of this article.)

7.3, and 1 mM PMSF. Complexes were concentrated using ultracentrifugation and loaded onto a HiLoad 26/60 Superdex 75 prep grade (GE Healthcare) size-exclusion column (SEC) to remove unbound or aggregated proteins prior to structural studies. Fractions were eluted in buffer containing 250 mM NaCl, 10 mM $CaCl_2$, 20 mM Hepes pH 7.3, and 1 mM PMSF. Samples containing complex were visualized by 15% native-PAGE, pooled, and concentrated to 0.5–1.0 mM using a centricon prior to experimental analyses.

2.2. NMR experiments

NMR experiments were performed on a Bruker Avance III 600 MHz spectrometer equipped with a conventional 5 mm probe. Samples consisting of [^{2}H, ^{15}N, ^{13}C] CaM, [^{2}H, ^{15}N, ^{13}C] CaM/CyaA-ACD, [^{2}H, ^{15}N, ^{13}C] CaM/CyaA-ACD(Q260C), and [^{2}H, ^{15}N, ^{13}C] CaM/CyaA-ACD(R262A) were suspended in buffer containing 250 mM NaCl, 10 mM $CaCl_2$, 20 mM Hepes pH 7.3, 1 mM PMSF, and 90%/H_2O/10% D_2O (NMR buffer) at a final concentration of 0.5–0.7 mM. Two dimensional Transverse Relaxation Optimized (^{1}H-^{15}N TROSY-HSQC) spectra were collected for all samples at 298 K [13]. CaM backbone assignments were determined in the presence and absence of CyaA-ACD using the following suite of triple-resonance experiments: HNCO, CBCA(CO)NH, HNCA, TROSY-HNCA, TROSY-HNCO, and NOESY-HSQC. NMR data were processed using NMRPipe [14] and analyzed using Sparky [15] Chemical-shift perturbations were calculated using Eq. (1)

$$\Delta\delta_{avg} = \sqrt{(\Delta\delta_H)^2 + \left(\frac{\Delta\delta_N}{5}\right)^2} \quad (1)$$

where $\Delta\delta_H$ and $\Delta\delta_N$ are the chemical shift differences between the amide proton–nitrogen resonances, respectively.

2.3. DLS experiments

DLS measurements were performed on samples suspended in NMR buffer at 20 μM using the Malvern Zetasizer instrument (Malvern) equipped with a temperature controller. Prior to recording DLS data, samples were centrifuged and filtered to remove particulate matter. Aliquots of 90 μl were dispensed into the small volume quartz cell and measurements were collected for CaM/CyaA-ACD and CaM/CyaA-ACD(Q260C) data sets. The temperature dependencies of the hydrodynamic radii were evaluated by increasing the temperature at 10 °C intervals from 25 °C to 70 °C. Data were analyzed using the Malvern Zetasizer software (Malvern).

3. Results and discussion

3.1. Conformational modulation of CaM upon CyaA-ACD association

We use NMR spectroscopy to investigate the interaction between CaM and CyaA-ACD at amino acid level resolution. Low solubility of free CyaA-ACD precludes NMR titration studies of its binding to CaM. As a consequence, our studies are focused on characterizing samples consisting of CaM/CyaA-ACD, CaM/CyaA-ACD(Q260C), or CaM/CyaA-ACD(R262A) complexes. The formation of equimolar CaM/CyaA-ACD complexes is monitored by native-PAGE and samples are subjected to SEC prior to NMR and DLS data

collection such that no unbound proteins are detectable (data not shown). Analysis of superimposed spectra of [^{2}H, ^{15}N, ^{13}C] CaM and [^{2}H, ^{15}N, ^{13}C] CaM/CyaA-ACD shows the formation of a homogeneous complex without the presence of detectable free CaM (Fig. 1). The association between free [^{2}H, ^{15}N, ^{13}C] CaM and [^{2}H, ^{15}N, ^{13}C] CaM/CyaA-ACD occurs in slow exchange on the NMR time scale as evidence by comparison of NMR spectra. NMR chemical shift assignments are achieved by analyses of 3D heteronuclear experiments recorded on free [^{2}H, ^{15}N, ^{13}C] CaM and complexes consisting of [^{2}H, ^{15}N, ^{13}C] CaM/CyaA-ACD, [^{2}H, ^{15}N, ^{13}C] CaM/CyaA-ACD(R262A), or [^{2}H, ^{15}N, ^{13}C] CaM/CyaA-ACD(Q260C); resonance assignments are determined for more than 85% of the non-proline residues in CaM for both the free and bound states.

Chemical shift perturbations between [^{2}H, ^{15}N, ^{13}C] CaM and [^{2}H, ^{15}N, ^{13}C] CaM/CyaA-ACD are monitored using 2D ^{1}H-^{15}N TROSY-HSQC spectra (Fig. 1A). NMR spectroscopy is useful in the determination of protein–protein binding interfaces and conformational modification of proteins induced by association with target ligands [16–19]. Comparison of amide-proton nitrogen correlation spectra of [^{2}H, ^{15}N, ^{13}C] CaM and [^{2}H, ^{15}N, ^{13}C] CaM/CyaA-ACD reveals structural perturbations occurring in both the N-CaM and C-CaM upon binding CyaA-ACD (Fig. 1B and C). The composite amide proton–nitrogen chemical differences plots are summarized for each amino acid residue in the ^{1}H–^{15}N TROSY-HSQC spectra (Fig. 2A). Most notably, larger perturbations are seen in residues from C-CaM as compared to N-CaM confirming that binding affinity is largely attributable to CyaA-ACD interaction with C-CaM as previously reported [20]. We observe conformational perturbations in residues F92 and V108 mapping to helices V and VI, respectively, which are known to interact extensively with helix H of CyaA-ACD. Additionally, residues K115, L116, and T117, located in the loop connecting helices VI and VII in C-CaM, experience conformational modification in response to CyaA-ACD binding (Fig. 1C). Movement of the VI–VII loop away from helices V and VIII is correlated with the structural transition induced by Ca^{2+}-binding to sites III and IV in CaM, which is known to increase the exposed hydrophobic surface area involved in target recognition [21–25]. Hydrophobic interactions between C-CaM and helix H of CyaA-ACD are reported to be important in complex formation [20]. The aromatic residue W242 of CyaA-ACD is buried in the hydrophobic pocket of C-CaM. In agreement with these findings, we observe significant chemical shift perturbations in the amide proton–nitrogen resonances of M109, M124, I125, A128, F141, and M144 located within the hydrophobic pocket of C-CaM. Methionine residues, known to play key roles in promoting diversity in target recognition by CaM, are important in the engagement of helix H in CyaA-ACD [20].

Smaller magnitude chemical shift perturbations are observed for amide proton–nitrogen resonances in N-CaM in the presence of CyaA-ACD, in particular for residues M36, M51, and M76 in the hydrophobic pocket (Fig. 2A). Indeed, the most prominent perturbations are localized to N-CaM residues A15, F16, G33, V35-S38, and R74 in helices I, II, and IV, respectively (Fig. 2A). NMR amide proton–nitrogen resonance shifts may be induced by direct contacts or by allosteric structural rearrangements. However, site-specific binding often promotes resonance broadening in NMR spectra as a consequence of the formation of larger sized protein complexes. Therefore, determining the ratio of amide proton–nitrogen peak intensities in the presence and absence of an effector is a powerful tool by which to distinguish direct and indirect binding events. Calculation of the ratios of amide proton–nitrogen peak intensities in the absence and presence of CyaA-ACD reveals that resonances mapping to C-CaM are significantly broadened, while those mapping to metal binding site I, the C-terminal region of helix I, and helix II of N-CaM experience moderate reductions in peak intensities (Fig. 2B–D) indicating that these regions likely

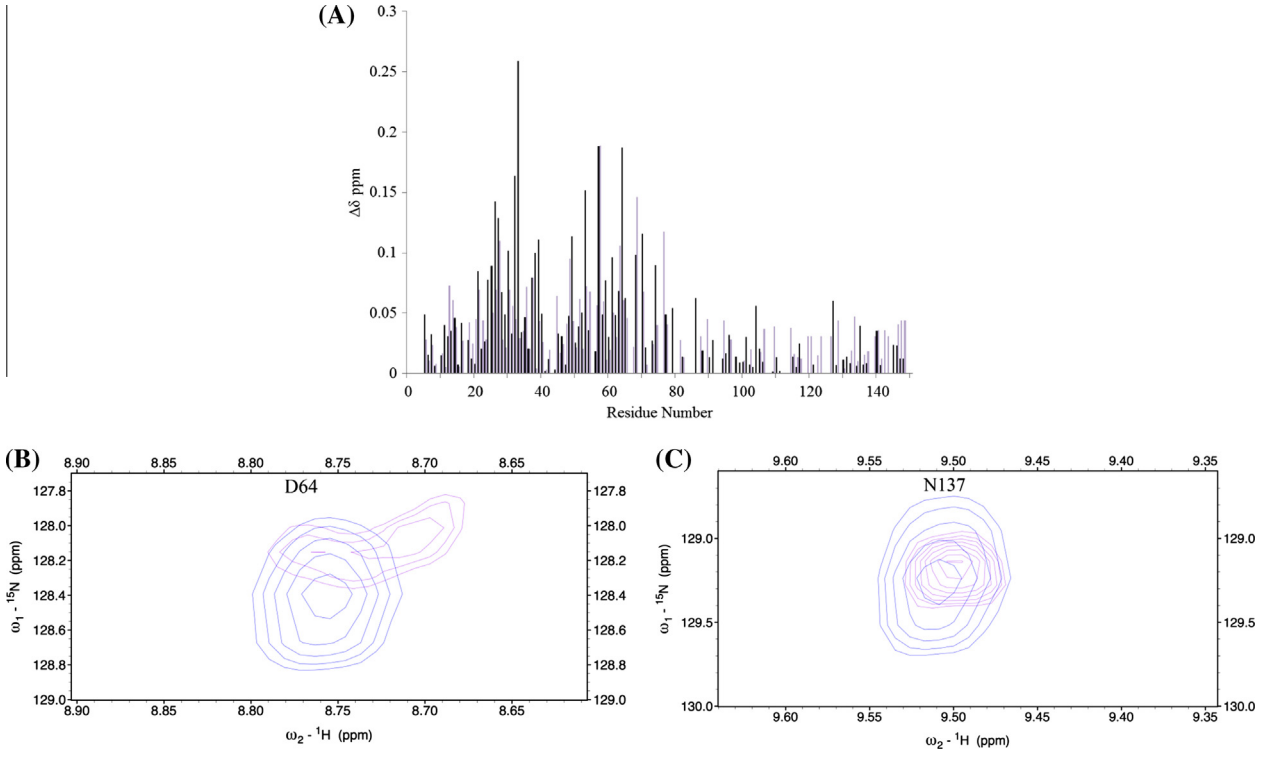

Fig. 3. Mapping the effects of β-hairpin mutation on CaM conformation. (A) Composite amide proton and nitrogen chemical shift differences between complexes consisting of [^{2}H, ^{15}N, ^{13}C] CaM/CyaA-ACD and [^{2}H, ^{15}N, ^{13}C] CaM/CyaA-ACD (Q260C) (purple bars) and of [^{2}H, ^{15}N, ^{13}C] CaM/CyaA-ACD and [^{2}H, ^{15}N, ^{13}C] CaM/CyaA-ACD (R262A) (black bars). (B, C) Specific N and C-terminal residues of [^{2}H, ^{15}N, ^{13}C] CaM/CyaA-ACD CaM/CyaA-ACD (blue) and [^{2}H, ^{15}N, ^{13}C] CaM/CyaA-ACD(Q260C) complexes (purple). (For interpretation of the references to color in this figure legend, the reader is referred to the web version of this article.)

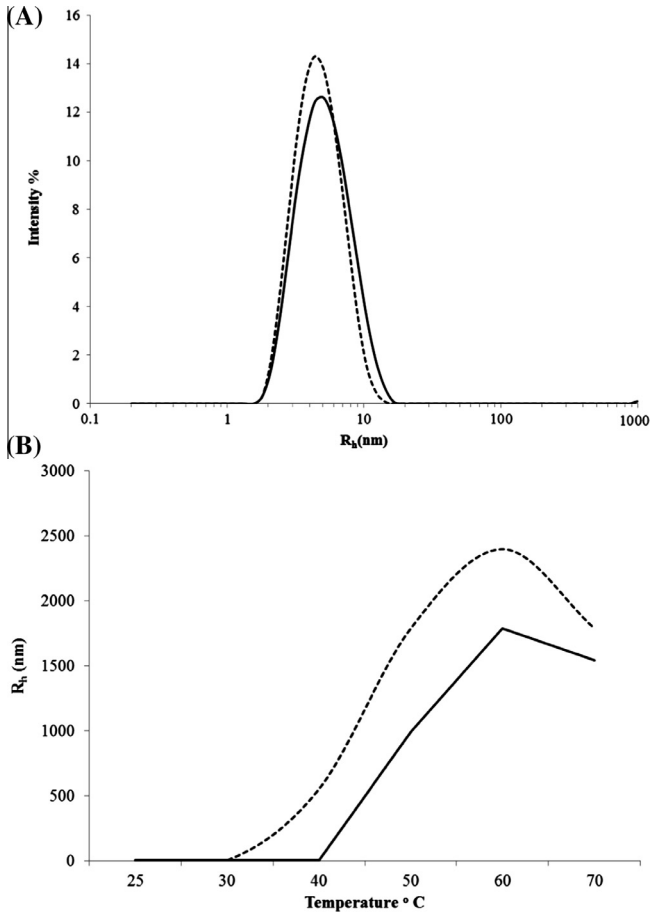

Fig. 4. Thermal stability of CaM/CyaA-ACD complexes. (A) DLS data comparing the hydrodynamic radii of CaM/CyaA-ACD (solid black line) and CaM/CyaA-ACD (Q260C) (dashed black line) complexes. (B) The R_h radii of CaM/CyaA-ACD (solid black line) and CaM/CyaA-ACD (Q260C) (dashed black line) complexes as a function of temperature. The reduced thermal stability of CaM/CyaA-ACD (Q260C) is evidence by aggregation at a lower temperature as compared to CaM/CyaA-ACD.

contact CyaA-ACD. Interestingly, resonances in the N-terminal region of site II are broadened in the complex, which correlates with previous reports of weak binding near metal binding site II [9], making it possible that communication between the metal binding sites is influenced by CyaA-ACD interaction. Based on the amide proton–nitrogen chemical shift values of CaM/CyaA-ACD, it is evident that the complex exhibits a unique conformation which is distinct from the Apo and Ca^{2+}-loaded states. Ulmer et al. [26] reported that interaction with EF modulates N-CaM structure and reduces metal affinity, possibly by preventing a structural transition in CaM to the fully open state. It is interesting to note that movement of helices I and IV has been linked to dynamic conformational exchange in N-CaM [27,28]. Therefore, it is conceivable that bacterial adenylate cyclase toxins uniquely interact with helices I and IV in CaM modifying the exchange between the "open" or "closed" states thereby offering a novel method by which to fine-tune metal affinity in CaM. Taken together, these data support that CyaA-ACD directly binds to both N-CaM and C-CaM which likely impacts CaM's metal sensing properties.

3.2. Configuration of CaM's metal-binding loops in the CyaA-ACD bound state

In this study, we report CyaA-ACD-dependent structural modulations occur in both N-CaM and C-CaM that involve the metal binding sites. In C-CaM, sites III and IV are structurally modified by interaction with CyaA-ACD. Comparison of NMR spectra demonstrates that the amide proton–nitrogen resonances for G96 and G98 are shifted downfield in the complex as compared to free CaM (Fig. 1A). The amides of G96 and G98 are hydrogen bonded to the carboxylate of D93, which forms part of the stabilizing network of hydrogen bonds in CaM's metal binding loops [21]. Given that there is a known relationship between hydrogen bonding strength and the magnitude of downfield chemical shifts in amide protons [29–31], it is likely that interaction with CyaA-ACD perturbs the hydrogen-bonding network in metal binding site III of CaM. In the crystal structure of C-CaM/CyaA-ACD, G96 is located within approximately 5.0 Å of R338 in CyaA-ACD. Similarly, G98 is located in close proximity to D360 and G361 in CyaA-ACD [20]. The amide proton–nitrogen chemical shifts of G96 and G98 may also be affected by the interaction of D93 with R338 in CyaA-ACD, which would further support that CyaA-ACD binding alters the hydrogen-bonding network of metal binding site III.

The amides of G132 and G134 are hydrogen bonded to the carboxylate side-chains of D129, interactions which stabilize the hydrogen-bonding network of metal-binding site IV of CaM in the free and CyaA-ACD bound states [20]. Additionally, the amide of G132 is hydrogen bonded to the backbone carbonyl of D129. In the spectrum of the CyaA-ACD complex, the amide proton–nitrogen resonances of G132 and G134 in CaM are shifted upfield (Fig. 1A), which may be indicative of weaker hydrogen bond strength and diminished interactions between the amides of G132 and G134 and the carboxylate side-chain of D129. Moreover, the carbonyl resonance of D129 is shifted upfield 0.3 ppm in the complex (data not shown), which may reflect the conformational consequences of A128 engaging W242 of CyaA-ACD. While G132, G134, or D129 do not directly associate with the toxin, insertion of W242 from CyaA-ACD into the hydrophobic pocket of CaM may also perturb the magnetic environment of resonances in site IV through the ring-current effects.

To probe the molecular interactions occurring between the β-hairpin and CaM, we compare the conformation of CaM/CyaA-ACD to complexes consisting of CaM/CyaA-ACD(Q260C) or CaM/CyaA(R262A) using 2D NMR. Mutation in the β-hairpin induces amide proton–nitrogen chemical shift perturbations localized to N-CaM, mainly in metal binding sites I and II, while C-CaM is largely unaffected (Fig. 3A). The apparent loss of interaction between N-CaM and CyaA-ACD promotes conformational exchange at metal binding site II (Fig. 3B), as evidenced by the observation of two peaks for this resonance mapping to site II, but C-CaM metal binding sites are unaffected (Fig. 3C). These findings indicate CyaA-ACD contacts N-CaM at or near the metal binding sites which likely modulates N-CaM's metal binding properties. Mutation of Q260 and R262 reduces maximal CaM-dependent activation in CyaA-ACD [9], functional consequences which our studies suggest may be influenced by structural changes in metal binding sites I and II, but the molecular mechanisms remain to be determined.

3.3. Global conformation and thermal stability of CaM/CyaA-ACD complexes

DLS is used to examine the global conformation of CaM/CyaA-ACD and CaM/CyaA-ACD(Q260C) complexes. At ambient temperatures, both complexes are homogeneous without the presence of detectable aggregates. Compared to free CaM, the CaM/CyaA-ACD complex is elongated with a Z-average R_h of 4.72 nm (Fig. 4A), which is consistent with that reported in the literature [20,32]. Upon mutation of the β-hairpin, the Z-average R_h of the complex decreases to 4.25 nm suggesting that loss of interaction with N-CaM induces a degree of compaction in the mutant complex. Analysis of the thermal dependencies of R_h reveals that CaM/

CyaA-ACD aggregates in solution above 40 °C (Fig. 4B). However, aggregation is noted at a lower temperature, above 30 °C in the CaM/CyaA-ACD(Q260C) complex, suggesting an overall reduction in the thermal stability of the mutant complex. Based on these findings, we submit that association of N-CaM with CyaA-ACD's β-hairpin promotes thermal stability in the complex.

In summary, our findings provide evidence demonstrating that both N-CaM and C-CaM are engaged upon CyaA-ACD binding. Our biophysical and structural studies reveal that CyaA-ACD binding modulates CaM's conformation, possibly through interactions mediated by association with its metal binding sites, and stabilizes formation of the enzyme complex. CaM-dependent stimulation of CyaA-ACD occurs in the presence and absence of elevated Ca^{2+} concentrations [5,33] suggesting that this enzyme has evolved a distinct manner of CaM-dependent activation. Our current structural studies seek to further elucidate sites of interaction between CaM and CyaA-ACD. The ultimate goal is to expand the mechanistic understanding of this potentially novel mode of CaM-dependent activation in a bacterial adenylate cyclase toxin.

Acknowledgments

We thank Dr. Vadim Gaponenko for the generous gift of the CaM plasmid and Dr. Wei-Jen Tang for the CyaA-ACD gene construct.

References

[1] J. Wolff, G.H. Cook, A.R. Goldhammer, S.A. Berkowitz, Calmodulin activates prokaryotic adenylate cyclase, Proc. Natl. Acad. Sci. U.S.A. 77 (1980) 3841–3844.
[2] D. Ladant, S. Michelson, R. Sarfati, A.M. Gilles, R. Predeleanu, O. Barzu, Characterization of the calmodulin-binding and of the catalytic domains of *Bordetella pertussis* adenylate cyclase, J. Biol. Chem. 264 (1989) 4015–4020.
[3] C.L. Weingart, P.S. Mobberley-Schuman, E.L. Hewlett, M.C. Gray, A.A. Weiss, Neutralizing antibodies to adenylate cyclase toxin promote phagocytosis of *Bordetella pertussis* by human neutrophils, Infect. Immun. 68 (2000) 7152–7155.
[4] A.A. Weiss, M.S. Goodwin, Lethal infection by *Bordetella pertussis* mutants in the infant mouse model, Infect. Immun. 57 (1989) 3757–3764.
[5] Y. Shen, Y.S. Lee, S. Soelaiman, P. Bergson, D. Lu, A. Chen, K. Beckingham, Z. Grabarek, M. Mrksich, W.J. Tang, Physiological calcium concentrations regulate calmodulin binding and catalysis of adenylyl cyclase exotoxins, EMBO J. 21 (2002) 6721–6732.
[6] C.L. Drum, Y. Shen, P.A. Rice, A. Bohm, W.J. Tang, Crystallization and preliminary X-ray study of the edema factor exotoxin adenylyl cyclase domain from *Bacillus anthracis* in the presence of its activator, calmodulin, Acta Crystallogr. D Biol. Crystallogr. 57 (2001) 1881–1884.
[7] C.L. Drum, S.Z. Yan, J. Bard, Y.Q. Shen, D. Lu, S. Soelaiman, Z. Grabarek, A. Bohm, W.J. Tang, Structural basis for the activation of anthrax adenylyl cyclase exotoxin by calmodulin, Nature 415 (2002) 396–402.
[8] V. Escuyer, E. Duflot, O. Sezer, A. Danchin, M. Mock, Structural homology between virulence-associated bacterial adenylate cyclases, Gene 71 (1988) 293–298.
[9] Q. Guo, J.E. Jureller, J.T. Warren, E. Solomaha, J. Florian, W.J. Tang, Protein–protein docking and analysis reveal that two homologous bacterial adenylyl cyclase toxins interact with calmodulin differently, J. Biol. Chem. 283 (2008) 23836–23845.
[10] H. Munier, F.J. Blanco, B. Precheur, E. Diesis, J.L. Nieto, C.T. Craescu, O. Barzu, Characterization of a synthetic calmodulin-binding peptide derived from *Bacillus anthracis* adenylate cyclase, J. Biol. Chem. 268 (1993) 1695–1701.
[11] E. Selwa, E. Laine, T.E. Malliavin, Differential role of calmodulin and calcium ions in the stabilization of the catalytic domain of adenyl cyclase CyaA from *Bordetella pertussis*, Proteins 80 (2012) 1028–1040.
[12] J.A. Putkey, G.R. Slaughter, A.R. Means, Bacterial expression and characterization of proteins derived from the chicken calmodulin cDNA and a calmodulin processed gene, J. Biol. Chem. 260 (1985) 4704–4712.
[13] M. Salzmann, K. Pervushin, G. Wider, H. Senn, K. Wuthrich, TROSY in triple-resonance experiments: new perspectives for sequential NMR assignment of large proteins, Proc. Natl. Acad. Sci. U.S.A. 95 (1998) 13585–13590.
[14] F. Delaglio, S. Grzesiek, G.W. Vuister, G. Zhu, J. Pfeifer, A. Bax, NMRPipe: a multidimensional spectral processing system based on UNIX pipes, J. Biomol. NMR 6 (1995) 277–293.
[15] T.D. Goddard, D.G. Kneller, Sparky-NMR Assignment and Integration Software, SPARKY 3, 2008.
[16] J.L. Urbauer, J.H. Short, L.K. Dow, A.J. Wand, Structural analysis of a novel interaction by calmodulin: high-affinity binding of a peptide in the absence of calcium, Biochemistry 34 (1995) 8099–8109.
[17] S. Grzesiek, S.J. Stahl, P.T. Wingfield, A. Bax, The CD4 determinant for downregulation by HIV-1 Nef directly binds to Nef. Mapping of the Nef binding surface by NMR, Biochemistry 35 (1996) 10256–10261.
[18] R.T. McKay, J.R. Pearlstone, D.C. Corson, S.M. Gagne, L.B. Smillie, B.D. Sykes, Structure and interaction site of the regulatory domain of troponin-C when complexed with the 96–148 region of troponin-I, Biochemistry 37 (1998) 12419–12430.
[19] N.J. Baxter, M.P. Williamson, Temperature dependence of ^{1}H chemical shifts in proteins, J. Biomol. NMR 9 (1997) 359–369.
[20] Q. Guo, Y. Shen, Y.S. Lee, C.S. Gibbs, M. Mrksich, W.J. Tang, Structural basis for the interaction of *Bordetella pertussis* adenylyl cyclase toxin with calmodulin, EMBO J. 24 (2005) 3190–3201.
[21] Y.S. Babu, C.E. Bugg, W.J. Cook, Structure of calmodulin refined at 2.2 A resolution, J. Mol. Biol. 204 (1988) 191–204.
[22] N.C. Strynadka, M.N. James, Crystal structures of the helix-loop-helix calcium-binding proteins, Annu. Rev. Biochem. 58 (1989) 951–998.
[23] M. Zhang, C. Abrams, L. Wang, A. Gizzi, L. He, R. Lin, Y. Chen, P.J. Loll, J.M. Pascal, J.F. Zhang, Structural basis for calmodulin as a dynamic calcium sensor, Structure 20 (2012) 911–923.
[24] H. Kuboniwa, N. Tjandra, S. Grzesiek, H. Ren, C.B. Klee, A. Bax, Solution structure of calcium-free calmodulin, Nat. Struct. Biol. 2 (1995) 768–776.
[25] M. Ikura, G.M. Clore, A.M. Gronenborn, G. Zhu, C.B. Klee, A. Bax, Solution structure of a calmodulin-target peptide complex by multidimensional NMR, Science 256 (1992) 632–638.
[26] T.S. Ulmer, S. Soelaiman, S. Li, C.B. Klee, W.J. Tang, A. Bax, Calcium dependence of the interaction between calmodulin and anthrax edema factor, J. Biol. Chem. 278 (2003) 29261–29266.
[27] D. Vigil, S.C. Gallagher, J. Trewhella, A.E. Garcia, Functional dynamics of the hydrophobic cleft in the N-domain of calmodulin, Biophys. J. 80 (2001) 2082–2092.
[28] S. Tripathi, J.J. Portman, Inherent flexibility determines the transition mechanisms of the EF-hands of calmodulin, Proc. Natl. Acad. Sci. U.S.A. 106 (2009) 2104–2109.
[29] G. Wagner, K. Wuthrich, Dynamics of protein structures, Naturwissenschaften 70 (1983) 105–114.
[30] T.K. Harris, A.S. Mildvan, High-precision measurement of hydrogen bond lengths in proteins by nuclear magnetic resonance methods, Proteins 35 (1999) 275–282.
[31] N.L. Finley, J.W. Howarth, P.R. Rosevear, Structure of the Mg^{2+}-loaded C-lobe of cardiac troponin C bound to the N-domain of cardiac troponin I: comparison with the Ca^{2+}-loaded structure, Biochemistry 43 (2004) 11371–11379.
[32] J.C. Karst, A.C. Sotomayor Perez, J.I. Guijarro, B. Raynal, A. Chenal, D. Ladant, Calmodulin-induced conformational and hydrodynamic changes in the catalytic domain of *Bordetella pertussis* adenylate cyclase toxin, Biochemistry 49 (2010) 318–328.
[33] D.V. Greenlee, T.J. Andreasen, D.R. Storm, Calcium-independent stimulation of *Bordetella pertussis* adenylate cyclase by calmodulin, Biochemistry 21 (1982) 2759–2764.